Beam-energy dependence of identified two-particle angular correlations in Au+Au collisions at RHIC

J. Adam,[6] L. Adamczyk,[2] J. R. Adams,[39] J. K. Adkins,[30] G. Agakishiev,[28] M. M. Aggarwal,[40] Z. Ahammed,[59] I. Alekseev,[3,35] D. M. Anderson,[53] A. Aparin,[28] E. C. Aschenauer,[6] M. U. Ashraf,[11] F. G. Atetalla,[29] A. Attri,[40] G. S. Averichev,[28] V. Bairathi,[22] K. Barish,[10] A. J. Bassill,[10] A. Behera,[51] R. Bellwied,[20] A. Bhasin,[27] J. Bielcik,[14] J. Bielcikova,[38] L. C. Bland,[6] I. G. Bordyuzhin,[3] J. D. Brandenburg,[48,6] A. V. Brandin,[35] J. Butterworth,[44] H. Caines,[62] M. Calderón de la Barca Sánchez,[8] D. Cebra,[8] I. Chakaberia,[29,6] P. Chaloupka,[14] B. K. Chan,[9] F-H. Chang,[37] Z. Chang,[6] N. Chankova-Bunzarova,[28] A. Chatterjee,[11] D. Chen,[10] J. H. Chen,[18] X. Chen,[47] J. Cheng,[55] M. Cherney,[13] M. Chevalier,[10] S. Choudhury,[18] W. Christie,[6] H. J. Crawford,[7] M. Csanád,[16] S. Das,[11] M. Daugherity,[1] T. G. Dedovich,[28] I. M. Deppner,[19] A. A. Derevschikov,[42] L. Didenko,[6] X. Dong,[31] J. L. Drachenberg,[1] J. C. Dunlop,[6] T. Edmonds,[43] N. Elsey,[61] J. Engelage,[7] G. Eppley,[44] R. Esha,[51] S. Esumi,[56] O. Evdokimov,[12] J. Ewigleben,[32] O. Eyser,[6] R. Fatemi,[30] S. Fazio,[6] P. Federic,[38] J. Fedorisin,[28] C. J. Feng,[37] Y. Feng,[43] P. Filip,[28] E. Finch,[50] Y. Fisyak,[6] A. Francisco,[62] L. Fulek,[2] C. A. Gagliardi,[53] T. Galatyuk,[15] F. Geurts,[44] A. Gibson,[58] K. Gopal,[23] D. Grosnick,[58] W. Guryn,[6] A. I. Hamad,[29] A. Hamed,[5] J. W. Harris,[62] W. He,[18] X. He,[26] S. Heppelmann,[8] S. Heppelmann,[41] N. Herrmann,[19] E. Hoffman,[20] L. Holub,[14] Y. Hong,[31] S. Horvat,[62] Y. Hu,[18] B. Huang,[12] H. Z. Huang,[9] S. L. Huang,[51] T. Huang,[37] X. Huang,[55] T. J. Humanic,[39] P. Huo,[51] G. Igo,[9] D. Isenhower,[1] W. W. Jacobs,[25] C. Jena,[23] A. Jentsch,[6] Y. JI,[47] J. Jia,[6,51] K. Jiang,[47] S. Jowzaee,[61] X. Ju,[47] E. G. Judd,[7] S. Kabana,[29] M. L. Kabir,[10] S. Kagamaster,[32] D. Kalinkin,[25] K. Kang,[55] D. Kapukchyan,[10] K. Kauder,[6] H. W. Ke,[6] D. Keane,[29] A. Kechechyan,[28] M. Kelsey,[31] Y. V. Khyzhniak,[35] D. P. Kikoła,[60] C. Kim,[10] D. Kincses,[16] T. A. Kinghorn,[8] I. Kisel,[17] A. Kiselev,[6] A. Kisiel,[60] M. Kocan,[14] L. Kochenda,[35] L. K. Kosarzewski,[14] L. Kramarik,[14] P. Kravtsov,[35] K. Krueger,[4] N. Kulathunga Mudiyanselage,[20] L. Kumar,[40] R. Kunnawalkam Elayavalli,[61] J. H. Kwasizur,[25] R. Lacey,[51] S. Lan,[11] J. M. Landgraf,[6] J. Lauret,[6] A. Lebedev,[6] R. Lednicky,[28] J. H. Lee,[6] Y. H. Leung,[31] C. Li,[47] W. Li,[49] W. Li,[44] X. Li,[47] Y. Li,[55] Y. Liang,[29] R. Licenik,[38] T. Lin,[53] Y. Lin,[11] M. A. Lisa,[39] F. Liu,[11] H. Liu,[25] P. Liu,[51] P. Liu,[49] T. Liu,[62] X. Liu,[39] Y. Liu,[53] Z. Liu,[47] T. Ljubicic,[6] W. J. Llope,[61] M. Lomnitz,[31] R. S. Longacre,[6] N. S. Lukow,[52] S. Luo,[12] X. Luo,[11] G. L. Ma,[49] L. Ma,[18] R. Ma,[6] Y. G. Ma,[49] N. Magdy,[12] R. Majka,[62] D. Mallick,[36] S. Margetis,[29] C. Markert,[54] H. S. Matis,[31] O. Matonoha,[14] J. A. Mazer,[45] K. Meehan,[8] J. C. Mei,[48] N. G. Minaev,[42] S. Mioduszewski,[53] B. Mohanty,[36] M. M. Mondal,[36] I. Mooney,[61] Z. Moravcova,[14] D. A. Morozov,[42] M. Nagy,[16] J. D. Nam,[52] Md. Nasim,[22] K. Nayak,[11] D. Neff,[9] J. M. Nelson,[7] D. B. Nemes,[62] M. Nie,[48] G. Nigmatkulov,[35] T. Niida,[61] L. V. Nogach,[42] T. Nonaka,[11] G. Odyniec,[31] A. Ogawa,[6] S. Oh,[62] V. A. Okorokov,[35] B. S. Page,[6] R. Pak,[6] A. Pandav,[36] Y. Panebratsev,[28] B. Pawlik,[2] D. Pawlowska,[60] H. Pei,[11] C. Perkins,[7] L. Pinsky,[20] R. L. Pintér,[16] J. Pluta,[60] J. Porter,[31] M. Posik,[52] N. K. Pruthi,[40] M. Przybycien,[2] J. Putschke,[61] H. Qiu,[26] A. Quintero,[52] S. K. Radhakrishnan,[29] S. Ramachandran,[30] R. L. Ray,[54] R. Reed,[32] H. G. Ritter,[31] J. B. Roberts,[44] O. V. Rogachevskiy,[28] J. L. Romero,[8] L. Ruan,[6] J. Rusnak,[38] O. Rusnakova,[14] N. R. Sahoo,[48] H. Sako,[56] S. Salur,[45] J. Sandweiss,[62] S. Sato,[56] W. B. Schmidke,[6] N. Schmitz,[33] B. R. Schweid,[51] F. Seck,[15] J. Seger,[13] M. Sergeeva,[9] R. Seto,[10] P. Seyboth,[33] N. Shah,[24] E. Shahaliev,[28] P. V. Shanmuganathan,[6] M. Shao,[47] F. Shen,[48] W. Q. Shen,[49] S. S. Shi,[11] Q. Y. Shou,[49] E. P. Sichtermann,[31] R. Sikora,[2] M. Simko,[38] J. Singh,[40] S. Singha,[26] N. Smirnov,[62] W. Solyst,[25] P. Sorensen,[6] H. M. Spinka,[4] B. Srivastava,[43] T. D. S. Stanislaus,[58] M. Stefaniak,[60] D. J. Stewart,[62] M. Strikhanov,[35] B. Stringfellow,[43] A. A. P. Suaide,[46] M. Sumbera,[38] B. Summa,[41] X. M. Sun,[11] Y. Sun,[47] Y. Sun,[21] B. Surrow,[52] D. N. Svirida,[3] P. Szymanski,[60] A. H. Tang,[6] Z. Tang,[47] A. Taranenko,[35] T. Tarnowsky,[34] J. H. Thomas,[31] A. R. Timmins,[20] D. Tlusty,[13] M. Tokarev,[28] C. A. Tomkiel,[32] S. Trentalange,[9] R. E. Tribble,[53] P. Tribedy,[6] S. K. Tripathy,[16] O. D. Tsai,[9] Z. Tu,[6] T. Ullrich,[6] D. G. Underwood,[4] I. Upsal,[48,6] G. Van Buren,[6] J. Vanek,[38] A. N. Vasiliev,[42] I. Vassiliev,[17] F. Videbæk,[6] S. Vokal,[28] S. A. Voloshin,[61] F. Wang,[43] G. Wang,[9] J. S. Wang,[21] P. Wang,[47] Y. Wang,[11] Y. Wang,[55] Z. Wang,[48] J. C. Webb,[6] P. C. Weidenkaff,[19] L. Wen,[9] G. D. Westfall,[34] H. Wieman,[31] S. W. Wissink,[25] R. Witt,[57] Y. Wu,[10] Z. G. Xiao,[55] G. Xie,[31] W. Xie,[43] H. Xu,[21] N. Xu,[31] Q. H. Xu,[48] Y. F. Xu,[49] Y. Xu,[48] Z. Xu,[6] Z. Xu,[9] C. Yang,[48] Q. Yang,[48] S. Yang,[6] Y. Yang,[37] Z. Yang,[11] Z. Ye,[44] Z. Ye,[12] L. Yi,[48] K. Yip,[6] H. Zbroszczyk,[60] W. Zha,[47] D. Zhang,[11] S. Zhang,[47] S. Zhang,[49] X. P. Zhang,[55] Y. Zhang,[47] Z. J. Zhang,[37] Z. Zhang,[6] J. Zhao,[43] C. Zhong,[49] C. Zhou,[49] X. Zhu,[55] Z. Zhu,[48] M. Zurek,[31] and M. Zyzak[17]

(STAR Collaboration)

[1] *Abilene Christian University, Abilene, Texas 79699*

[2] *AGH University of Science and Technology, FPACS, Cracow 30-059, Poland*

[3] *Alikhanov Institute for Theoretical and Experimental Physics NRC "Kurchatov Institute", Moscow 117218, Russia*

[4] *Argonne National Laboratory, Argonne, Illinois 60439*
[5] *American University of Cairo, New Cairo 11835, New Cairo, Egypt*
[6] *Brookhaven National Laboratory, Upton, New York 11973*
[7] *University of California, Berkeley, California 94720*
[8] *University of California, Davis, California 95616*
[9] *University of California, Los Angeles, California 90095*
[10] *University of California, Riverside, California 92521*
[11] *Central China Normal University, Wuhan, Hubei 430079*
[12] *University of Illinois at Chicago, Chicago, Illinois 60607*
[13] *Creighton University, Omaha, Nebraska 68178*
[14] *Czech Technical University in Prague, FNSPE, Prague 115 19, Czech Republic*
[15] *Technische Universität Darmstadt, Darmstadt 64289, Germany*
[16] *ELTE Eötvös Loránd University, Budapest, Hungary H-1117*
[17] *Frankfurt Institute for Advanced Studies FIAS, Frankfurt 60438, Germany*
[18] *Fudan University, Shanghai, 200433*
[19] *University of Heidelberg, Heidelberg 69120, Germany*
[20] *University of Houston, Houston, Texas 77204*
[21] *Huzhou University, Huzhou, Zhejiang 313000*
[22] *Indian Institute of Science Education and Research (IISER), Berhampur 760010 , India*
[23] *Indian Institute of Science Education and Research (IISER) Tirupati, Tirupati 517507, India*
[24] *Indian Institute Technology, Patna, Bihar 801106, India*
[25] *Indiana University, Bloomington, Indiana 47408*
[26] *Institute of Modern Physics, Chinese Academy of Sciences, Lanzhou, Gansu 730000*
[27] *University of Jammu, Jammu 180001, India*
[28] *Joint Institute for Nuclear Research, Dubna 141 980, Russia*
[29] *Kent State University, Kent, Ohio 44242*
[30] *University of Kentucky, Lexington, Kentucky 40506-0055*
[31] *Lawrence Berkeley National Laboratory, Berkeley, California 94720*
[32] *Lehigh University, Bethlehem, Pennsylvania 18015*
[33] *Max-Planck-Institut für Physik, Munich 80805, Germany*
[34] *Michigan State University, East Lansing, Michigan 48824*
[35] *National Research Nuclear University MEPhI, Moscow 115409, Russia*
[36] *National Institute of Science Education and Research, HBNI, Jatni 752050, India*
[37] *National Cheng Kung University, Tainan 70101*
[38] *Nuclear Physics Institute of the CAS, Rez 250 68, Czech Republic*
[39] *Ohio State University, Columbus, Ohio 43210*
[40] *Panjab University, Chandigarh 160014, India*
[41] *Pennsylvania State University, University Park, Pennsylvania 16802*
[42] *NRC "Kurchatov Institute", Institute of High Energy Physics, Protvino 142281, Russia*
[43] *Purdue University, West Lafayette, Indiana 47907*
[44] *Rice University, Houston, Texas 77251*
[45] *Rutgers University, Piscataway, New Jersey 08854*
[46] *Universidade de São Paulo, São Paulo, Brazil 05314-970*
[47] *University of Science and Technology of China, Hefei, Anhui 230026*
[48] *Shandong University, Qingdao, Shandong 266237*
[49] *Shanghai Institute of Applied Physics, Chinese Academy of Sciences, Shanghai 201800*
[50] *Southern Connecticut State University, New Haven, Connecticut 06515*
[51] *State University of New York, Stony Brook, New York 11794*
[52] *Temple University, Philadelphia, Pennsylvania 19122*
[53] *Texas A&M University, College Station, Texas 77843*
[54] *University of Texas, Austin, Texas 78712*
[55] *Tsinghua University, Beijing 100084*
[56] *University of Tsukuba, Tsukuba, Ibaraki 305-8571, Japan*
[57] *United States Naval Academy, Annapolis, Maryland 21402*
[58] *Valparaiso University, Valparaiso, Indiana 46383*
[59] *Variable Energy Cyclotron Centre, Kolkata 700064, India*
[60] *Warsaw University of Technology, Warsaw 00-661, Poland*
[61] *Wayne State University, Detroit, Michigan 48201*
[62] *Yale University, New Haven, Connecticut 06520*

(Dated: October 30, 2019)

The two-particle angular correlation functions, R_2, of pions, kaons, and protons in Au+Au collisions at $\sqrt{s_{NN}}$ = 7.7, 11.5, 14.5, 19.6, 27, 39, 62.4, and 200 GeV were measured by the STAR experiment at RHIC. These correlations were measured for both like-sign and unlike-sign charge

combinations and versus the centrality. The correlations of pions and kaons show the expected near-side (*i.e.*, at small relative angles) peak resulting from short-range mechanisms. The amplitudes of these short-range correlations decrease with increasing beam energy. However, the proton correlation functions exhibit strong anticorrelations in the near-side region. This behavior is observed for the first time in an A+A collision system. The observed anticorrelation is p_T-independent and decreases with increasing beam energy and centrality. The experimental results are also compared to the Monte Carlo models UrQMD, Hijing, and AMPT.

PACS numbers: 25.75.-q, 25.75.Gz

I. INTRODUCTION

The study of single-particle observables provides information on the bulk properties of the hot nuclear systems formed in relativistic heavy-ion collisions. A more differential view, first employed to understand the systems produced at the ISR in the 1970's [1–4], involves the use of two-particle correlators. Here, one measures the rates for all pairs of particles in single events versus kinematic observables in two dimensions, *e.g.*, the relative rapidity and azimuthal angle, $(\Delta y, \Delta\varphi)$, of the two particles in each pair. These distributions can then be normalized by the distributions formed once the intraevent correlations have been explicitly broken. This normalization also removes any contributions to the correlators from all single-particle inefficiencies in the experimental measurement. The resulting ratio, called R_2, then depicts excesses or deficits with respect to unity that directly indicate correlations or anticorrelations, respectively. Parton fragmentation, resonance decays, and femtoscopic correlations, typically referred to as "short-range" correlations, are localized to a narrow region near $(\Delta y, \Delta\varphi) \sim 0$ [5, 6]. Other phenomena are longer range, such as elliptic flow, which appear as a cosine function of the relative azimuthal angle [7]. Global momentum conservation can result in a back-to-back correlation between the produced particles, which is reflected as a negative cosine function of $\Delta\varphi$ [7–9]. Non-zero integrals of the two-particle correlation functions result in multiplicity distributions with variances that are not equal to the mean values, as would be expected for purely Poisson fluctuations. As the variance of the multiplicity distributions goes like the square of the correlation length [10], the two-particle correlation functions thus provide a more differential view of effects which may potentially result from the proximity of a critical point [10–16]. Such a critical point would be expected to mark the end of the first-order phase transition line separating hadronic and partonic matter. The expected critical point signal is thus a nonmonotonic dependence of the fluctuations and correlations on the beam energy. Therefore, multiparticle correlations, and their integrals the fluctuations, deserve careful study.

In this paper, the two-particle correlations are studied for like-sign and unlike-sign identified pions, kaons, and protons in Au+Au collisions measured by the STAR experiment during the Beam Energy Scan (BES) program at RHIC. The angular correlation functions are presented at eight different beam energies ranging from 7.7 to 200 GeV and at three selected centralities, the most central 0%-5%, 30%-40%, and peripheral 60%-70%. Two ranges of low and high transverse momentum are also compared. The study of the different particle species pairs allows one to compare the meson (π and K) and baryon (p) correlations. The beam energy dependence spans nearly baryon-free matter at the highest energy to increasingly baryon-doped matter as the beam energy is decreased. The experimental results are also compared to those from the models UrQMD [17], Hijing [18], and AMPT [19], each of which produces events based on different theoretical approaches.

This paper is organized as follows: the STAR detector and other experimental details are described in Section II; the two-particle angular correlation function results are presented in Section III. Finally, the summary and conclusions are presented in Section IV.

II. EXPERIMENTAL DETAILS

The Solenoidal Tracker at RHIC (STAR) is an azimuthally-symmetric and wide acceptance detector. The key subdetectors used here include the Time Projection Chamber (TPC) [20], which performs the track and primary vertex reconstruction, as well as particle identification at low momentum, and the Time-of-Flight system (TOF) [21], which provides particle identification information at higher momentum. A solenoidal magnet aligned with the beam axis provides a uniform magnetic field of 0.5 T for charged particle momentum analysis [22].

The data studied here were collected in the years 2010, 2011, and 2014, and include the eight beam energies of $\sqrt{s_{NN}}$ = 7.7, 11.5, 14.5, 19.6, 27, 39, 62.4, and 200 GeV. These data were collected with a minimum bias trigger based on the information from the Vertex Position Detector (VPD) [23], Beam-Beam Counters (BBC) and Zero Degree Calorimeter (ZDC) detectors [24]. The raw event totals and the year of data collection are shown in Table I.

The collision vertex, determined using all charged tracks in each event, was required to be within ±30 cm of the center of STAR along the beam direction at all eight beam energies. Pseudocorrelations caused by the event by event variation of the location of the primary vertex along the beam pipe, Z_{vtx}, were removed by performing the analyses in 30 bins of Z_{vtx}, each 2 cm wide. A

TABLE I: The number of events and year the data was taken versus the beam energy.

$\sqrt{s_{NN}}$ (GeV)	Year	N_{events} (million)
7.7	2010	3.2
11.5	2010	11.4
14.5	2014	15.9
19.6	2011	17.1
27	2011	31.3
39	2010	36.8
62.4	2010	39
200	2010	59.3

weighted average of the correlation functions over these bins was then constructed, eliminating these pseudocorrelations [25].

For the pion or kaon correlations, the centrality of the collisions was determined using the charged particle multiplicity distributions with pseudorapidities, η, within the range $0.5 < |\eta| < 1$ and a Monte Carlo Glauber simulation as described, *e.g.*, in Ref. [26]. For the proton correlations, the centrality was determined using the measured multiplicity of tracks, excluding protons, with $|\eta| < 1$. These same centrality definitions were used in the STAR papers on the multiplicity cumulants [27–29]. To avoid artifacts in the observables of interest caused by the above multiplicity binning on pseudorapidity, the correlation functions were studied only for pseudorapidities within the range $|\eta| < 0.5$.

The raw events collected by STAR were then pruned of data-taking runs in which the average values of a number of observables deviated by two standard deviations from their values over all events. Examples of the variables studied are the mean values of several different track or hit multiplicities, or the average values of track-based quantities such as the transverse momentum or azimuthal angle. About thirty such variables were studied in each run, and the most sensitive to "bad runs" were generally the number of primary reconstructed tracks per event, the number of tracks per event that matched to TOF hits, the east-west asymmetry in the track pseudorapidity, and the averages of the track transverse and total momentum. Once the bad runs were removed, multiple selection criteria on pairs of global observables were applied to remove bad events in good runs. These selection criteria were effective at removing collisions of gold nuclei with beam line materials (most importantly at the lowest beam energies) and collision pile-up in time in the TPC (most importantly at the highest beam energies). The tracks used in the correlations analyses were subject to quality cuts on the distance of closest approach to the primary vertex (maximum 2 cm), the number of TPC space points assigned to each track (minimum 18), and the ratio of assigned to total possible space points (minimum 52%).

The correlation functions were measured using like-sign (LS) and unlike-sign (US) pairs of pions, kaons, and protons, separately. The kinematic acceptance used for the different particle species is shown in Table II. To identify the particles, the ionization energy loss, dE/dx, measured by the TPC and the time of flight measured by the TOF detector was used. The dE/dx selection was done within two standard deviations of each particle's peak in the normalized ionization energy loss distributions. The TOF efficiency per TPC track is ∼60-70%. If the TOF information was available for a given TPC track, a cut was placed on the mass obtained from the track momentum and speed. If a particular track did not have TOF information, additional exclusionary dE/dx cuts on nearby particle species were applied at low momenta.

TABLE II: The kinematic acceptance in rapidity and transverse momentum for pions, kaons, and protons in this analysis.

$\pi^{\pm}$	$0.2<p_T<2.0$ GeV/c	$\|y\|<0.42$
$K^{\pm}$	$0.2<p_T<1.6$ GeV/c	$\|y\|<0.40$
p,$\bar{\text{p}}$	$0.4<p_T<2.0$ GeV/c	$\|y\|<0.60$

By definition, the correlation functions, R_2, are insensitive to single-particle experimental inefficiencies caused, for example, by gaps in the detector. However, "track crossing," a true two-particle inefficiency, remains. The track reconstruction algorithm used in STAR does not share space points between two nearby tracks. The imposition of even minimal quality cuts on the number of space points assigned to a reconstructed track thus causes one of the tracks in the pair to have fewer space points and thus a slightly lower efficiency. This relative inefficiency for finding a track because of the existence of another nearby creates a "near-side," $(\Delta y, \Delta\varphi) \sim 0$, hole in the correlation functions. This was avoided in the present analysis by p_T-ordering the particles in each pair to constrain the track crossing inefficiency to a smaller region, then reflecting the unaffected bins across $\Delta\varphi = \Delta y = 0$ to form the correlation functions devoid of track crossing [25]. The affected regions for each particle species are summarized in Table III. Additional systematic uncertainties result from the specific treatment of the track crossing inefficiency and these can be seen in the results below for the few bins very close to $\Delta y = 0$.

TABLE III: The kinematic regions affected by the track crossing inefficiency and subsequent correction for each particle species.

$\pi^{\pm}$	$\|\Delta y\| < 0.09$	LS: $-5^\circ < \|\Delta\varphi\| < 35^\circ$
		US: $-85^\circ < \|\Delta\varphi\| < -5^\circ$
$K^{\pm}$	$\|\Delta y\| < 0.12$	LS: $-5^\circ < \|\Delta\varphi\| < 35^\circ$
		US: $-85^\circ < \|\Delta\varphi\| < -5^\circ$
p,$\bar{\text{p}}$	$\|\Delta y\| < 0.20$	LS: $-5^\circ < \|\Delta\varphi\| < 25^\circ$
		US: $-35^\circ < \|\Delta\varphi\| < -5^\circ$

A. Two-particle angular correlation functions

The correlation function is defined as the ratio of the two-particle density distributions and the product, or convolution, of the single-particle densities. This division normalizes the correlations as "per pair," and makes them insensitive to single-particle reconstruction and acceptance inefficiencies [1, 16, 30]. The normalized "angular correlations," R_2, are formed as a function of the relative rapidity and azimuthal angle of the two particles in the pair, $(\Delta y, \Delta\varphi)$, and are given by [1, 2, 16, 30–32]:

$$R_2(\Delta y, \Delta\varphi) = \frac{\rho_2(\Delta y, \Delta\varphi)}{\rho_1(y_1, \varphi_1)\rho_1(y_2, \varphi_2)} - 1, \qquad (1)$$

where $\Delta y = y_1 - y_2$, $\Delta\varphi = \varphi_1 - \varphi_2$, and $\rho_2(\Delta y, \Delta\varphi)$ and $\rho_1(y, \varphi)$ are the two-particle and single-particle multiplicity density distributions, respectively, normalized to the number of events.

The numerator of the correlation functions for particles is calculated using all pairs in each event except self-pairs. Several methods are available to calculate the denominator. These include pulling particles of interest from two different but similar events, which is called "mixing," and convolution. In convolution, a single-particle spectrum versus (y, φ, p_T) is folded with itself in six nested loops to produce the denominator versus the pair $(\Delta y, \Delta\varphi)$. This six-dimension convolution allows one to impose the same cut (see previous section) in the denominator as was used in the numerator to remove the two-particle inefficiency from track crossing. The results from the two methods to form the denominator, mixing and convolution, were found to be in excellent agreement.

The amplitudes of such R_2 correlation functions often decrease with increasing beam energy and/or centrality as a result of the increasing number of particle-emitting sources for higher-energy (and/or more central) collisions. One may thus consider scaling the correlators with some multiplicity such as the number of participants or binary collisions to account for such dilution. The correlators shown here do not include such an additional scaling.

In the present analysis, the numerator and denominator of the correlation functions were further normalized to the event-averaged number of pairs [1] via,

$$R_2(\Delta y, \Delta\varphi) = \frac{\langle n\rangle^2}{\langle n(n-1)\rangle} \frac{\rho_2(\Delta y, \Delta\varphi)}{\rho_1(y_1, \varphi_1)\rho_1(y_2, \varphi_2)} - 1, \quad (2)$$

where n is the event-by-event multiplicity of the indistinguishable particle of interest in a given centrality and Z_{vtx} bin. If the particles in the pair are distinguishable, this prefactor becomes $\langle n_1\rangle\langle n_2\rangle/\langle n_1 n_2\rangle$, where n_1 and n_2 are the event-wise multiplicities of the distinguishable particles of interest. This normalization removes purely mathematical finite-multiplicity offsets to the correlation functions and thus ensures that the values of R_2 are identically zero in the absence of any two-particle (anti)correlations even at low multiplicities of the particle of interest in each event.

B. Systematic uncertainty

To estimate the systematic uncertainties, the track selection and particle identification criteria were modified within reasonable ranges, and the full analysis was repeated for each cuts set. The systematic uncertainties for the track selection and particle identification were separately studied. The standard deviation of the results when using the default cut was calculated for each set and the systematic uncertainty was determined as the root of the quadratic sum of the different systematic sources.

The main source of systematic uncertainty for the pion results was the cut on the distance of closest approach to the primary vertex. For the kaon and proton results, the particle identification cuts resulted in the largest contributions in the systematic uncertainties. The absolute uncertainties of the main systematic source averaged over Δy at 62.4 GeV, 30%-40% centrality, were found to be 0.1×10^{-3} for like-sign and unlike-sign pions, 0.3×10^{-3} for like-sign kaons and protons, and lower than 0.5×10^{-3} for unlike-sign kaons and protons. The systematic uncertainties at 14.5 GeV, and 30%-40% centrality, are similar, although they increase to 0.8×10^{-3} for like-sign kaons, and 0.1×10^{-2} for unlike-sign kaons and protons. The final source of systematic uncertainty results from the necessary correction for the track crossing pair inefficiency. This contribution can be larger than the other systematics but only for the few bins near $\Delta y = 0$, as will be seen in the results presented below.

III. RESULTS

The angular correlation functions for like-sign and unlike-sign identified π mesons and protons are shown in Fig. 1 and 2, respectively, for the eight different energies and for 30%-40% mid-central collisions. The kaon correlations are shown in Fig. 3 at 200 GeV and 30%-40% centrality. The kaon correlations at lower energies are similar, but become increasingly noisy due to the weakening production of kaons (and the fewer number of experimental events) as the energy is decreased.

The like-sign correlations for pions and kaons are the average of the like-sign positive and like-sign negative correlation functions. For protons, the like-sign positive and like-sign negative are separately studied. The like-sign antiproton correlation functions are statistically significant only at the highest beam energies.

The correlation functions shown in Figs. 1-3 reflect the different physical mechanisms occurring in Au+Au collisions at 30%-40% centrality. Energy-momentum conservation and dijet fragmentation generally contribute to produce the away-side ridge at $\Delta\varphi \sim 180°$, and collective elliptic flow is responsible for the double ridge structure at $\Delta\varphi = 0°$ and 180°. These general features depend weakly on the beam energy for both the like-sign and unlike-sign charge combinations. The correlations of pions and kaons exhibit a peak at $(\Delta y, \Delta\varphi) \sim 0$

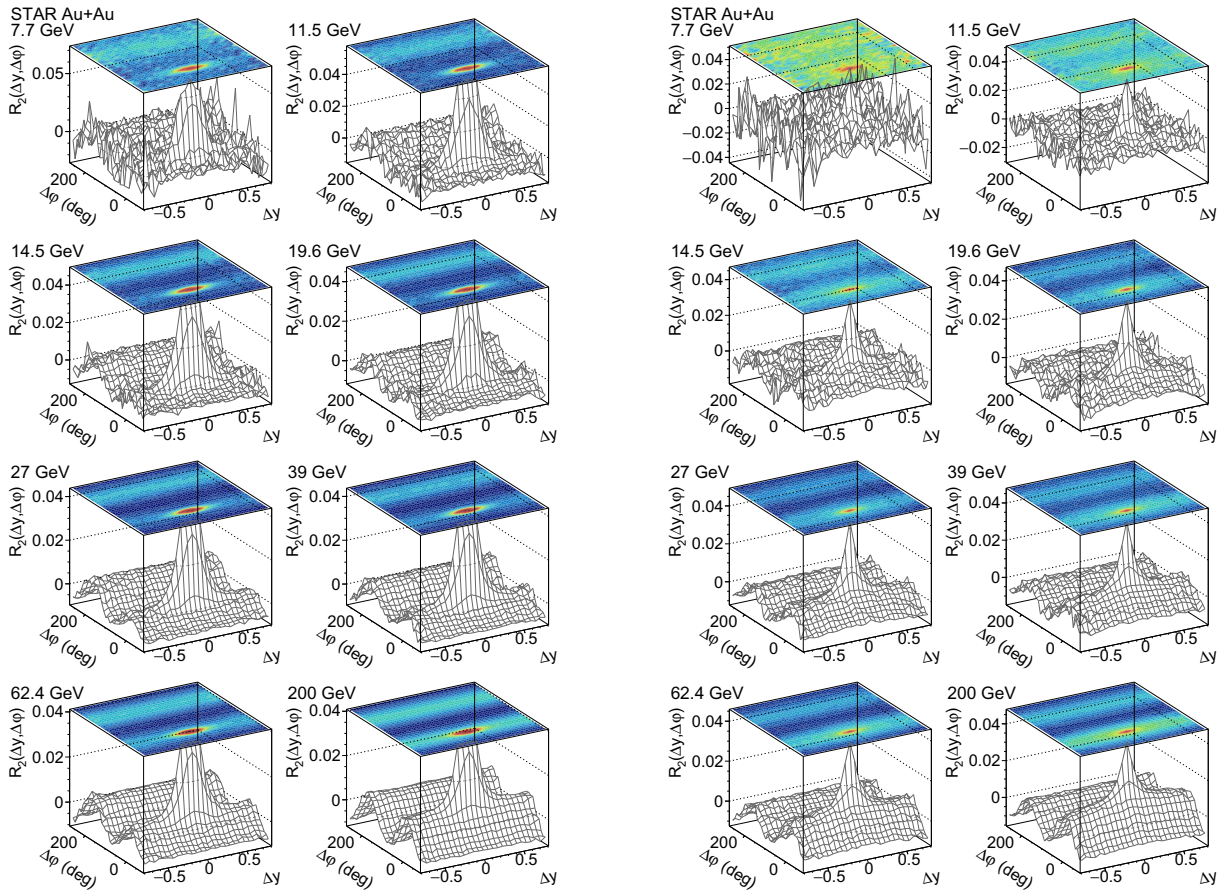

(a) Like-sign pions

(b) Unlike-sign pions

FIG. 1: Angular correlation function $R_2(\Delta y, \Delta\varphi)$ of like-sign (left) and unlike-sign (right) pions in Au+Au collisions at mid centrality 30%-40% and $0.2 < p_T < 2.0$ GeV/c in different beam energies from 7.7 GeV (top left) to 200 GeV (bottom right).

that would typically be associated with the short-range mechanisms of minijet string breaking, femtoscopic correlations, and resonance decay. Femtoscopic correlations include quantum-statistical effects, Coulomb, and strong interactions and can be positive or negative.

The strong near side peaks in the like-sign two-pion correlations shown in Fig. 1 ($p_T < 2$ GeV/c) are predominantly femtoscopic in nature. These peaks can be cleanly excised by removing the (very small) fraction of pairs with $\Delta q < 100$ MeV/c, where Δq is the modulus of the energy-momentum four-vector difference of the two particles in each pair. Such a cut has very little effect on the unlike-sign pion correlations because quantum-statistical effects do not occur for distinguishable particles.

The near-side peak in the unlike-sign kaon correlations is wider in $(\Delta y, \Delta\varphi)$ compared to the like-sign kaons in Fig. 3. This near-side correlation in unlike-sign kaons is in the shape of a caldera centered at $(\Delta y, \Delta\varphi) \sim 0$ which results from K^+K^- pairs that are the daughters of $\phi(1020)$ mesons [33, 34].

The proton correlation functions are qualitatively similar to those for pions and kaons on the away side in $\Delta\varphi$. However, a significant difference is observed on the near side, $(\Delta y, \Delta\varphi) \sim 0$. The values of the like-sign proton correlation functions show a wide suppression on the near side. Upon this wide anticorrelation may sit a narrow peak at $(\Delta y, \Delta\varphi) \sim 0$.

For the unlike-sign proton pairs, a prominent near-side ridge along the Δy axis is observed for the larger values of Δy. At smaller values of Δy, a clear anticorrelation with respect to this ridge is observed. This anticorrelation in unlike-sign proton pairs near $(\Delta y, \Delta\varphi) \sim 0$ is narrower in Δy than the near-side anticorrelation observed for the like-sign proton pairs.

The projections of the angular correlation functions onto the Δy axis (integrated over all azimuthal angles) for like-sign and unlike-sign pion and proton pairs in 30%-40% central collisions are shown in Fig. 4. The proton pair correlations and pion pair correlations differ significantly at all eight energies and for both like-sign and unlike-sign combinations. The pion correlations show an enhancement around $\Delta y \sim 0$ which decreases slightly with increasing beam energy.

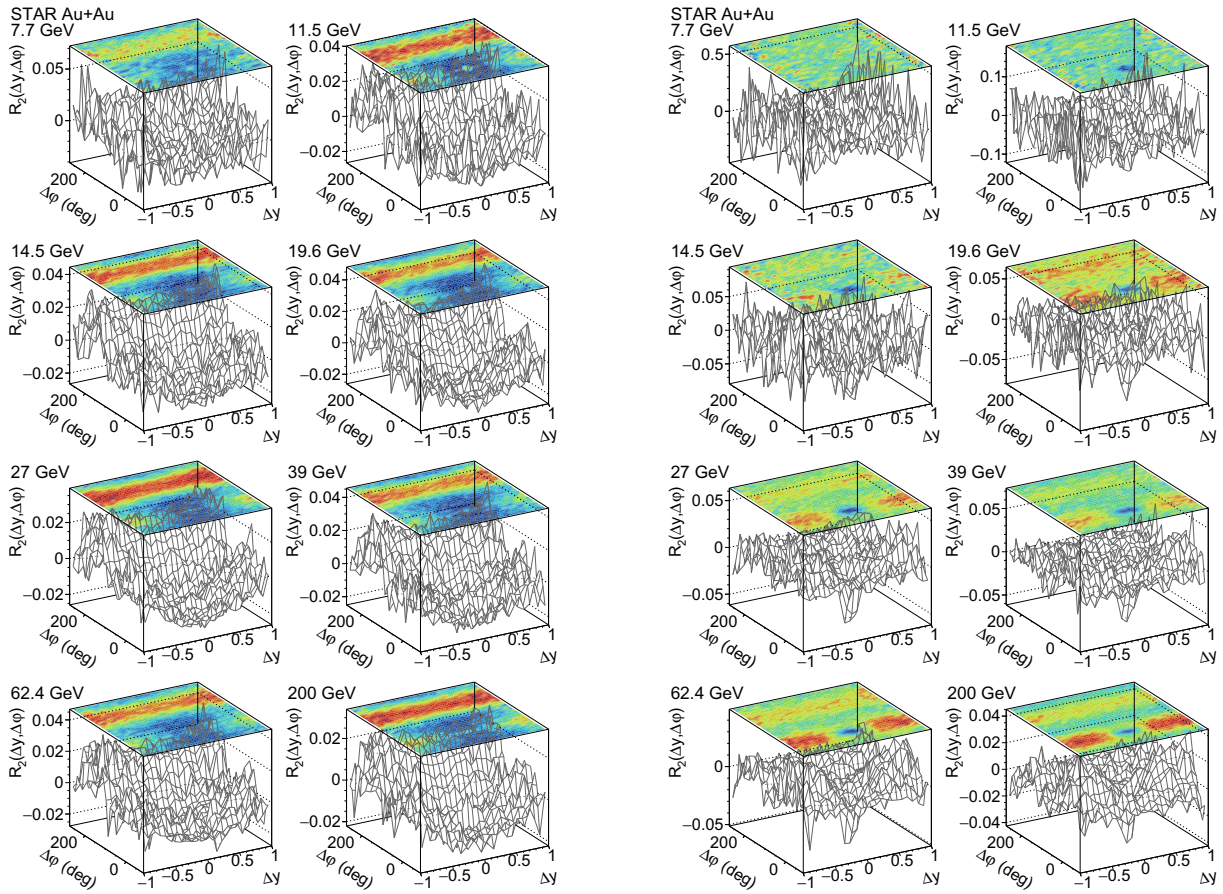

(a) Like-sign protons

(b) Unlike-sign protons

FIG. 2: Angular correlation function $R_2(\Delta y, \Delta\varphi)$ of like-sign (left) and unlike-sign (right) protons in Au+Au collisions at mid centrality 30%-40% and $0.4 < p_T < 2.0$ GeV/c in different beam energies from 7.7 GeV (top left) to 200 GeV (bottom right). Due to the large statistical fluctuations in large Δy bins, the plots are presented in the range of $|\Delta y| \leq 1$.

In contrast, both the like-sign and unlike-sign proton correlations show an anticorrelation near $\Delta y \sim 0$ at all eight energies. These anticorrelations are remarkably weakly-dependent on the beam energy. The values of the correlation functions near $\Delta y \sim 0$ for the like-sign (red) and unlike-sign (blue) pairs are comparable at all eight energies. At larger values of the rapidity difference, the like-sign proton correlations continue to rise roughly linearly, while the values for unlike-sign pairs level off to form the near-side ridge seen in Fig. 2.

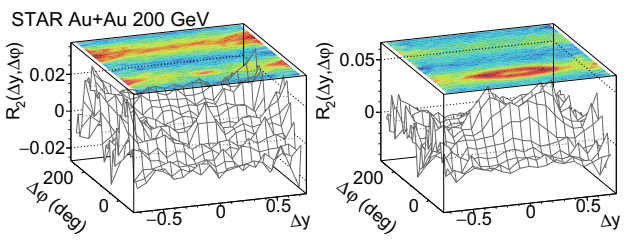

FIG. 3: Angular correlation function $R_2(\Delta y, \Delta\varphi)$ of like-sign (left) and unlike-sign (right) kaons in Au+Au collisions at 200 GeV, mid centrality 30%-40% and $0.2 < p_T < 1.6$ GeV/c.

Also shown on the lower right in this figure are the like-sign antiproton correlation functions (green) at the two highest beam energies. Lower beam energies result in considerably fewer antiprotons, and thus much more uncertain correlation functions, so the like-sign antiproton results are not shown for clarity. The like-sign antiproton correlations are consistent with those for like-sign protons.

The projection of $R_2(\Delta y, \Delta\varphi)$ into Δy, averaged over $|\Delta\varphi| < 85°$ (a "near-side projection") or averaged over $85° \leq |\Delta\varphi| \leq 275°$ (an "away-side projection") is shown in Fig. 5 for the like-sign and unlike-sign pion and proton pairs at 14.5 and 62.4 GeV in 30%-40% central collisions. The away-side projections of the pion and proton correlations are roughly flat versus the rapidity difference as seen in the two right frames of Figs. 5a and 5b. There is a slight suppression on the away-side for the like-sign protons due to the wider near-side anticorrelation in

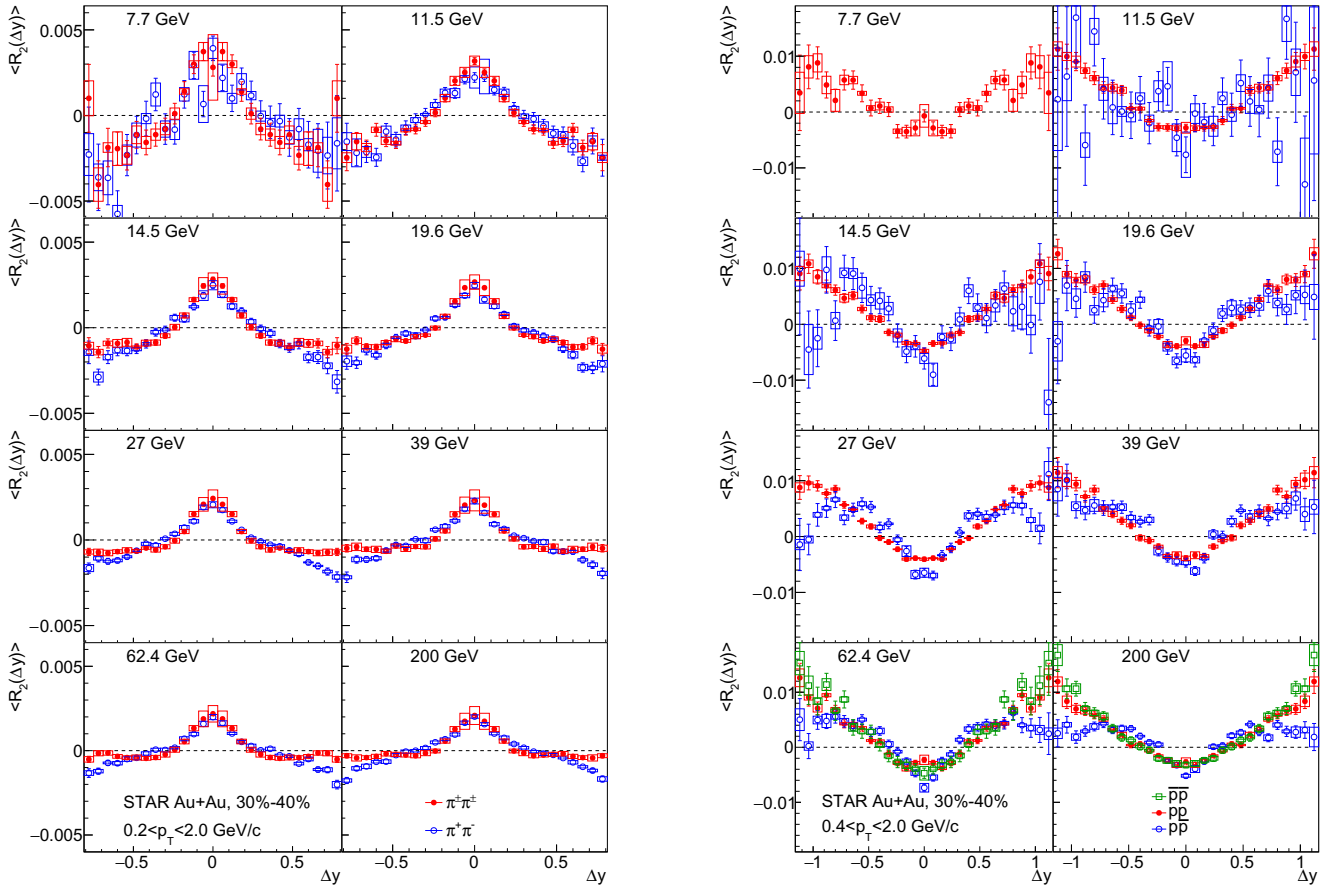

(a) pions (b) protons

FIG. 4: Projection of correlation function $\langle R_2(\Delta y)\rangle$ of like-sign (red) and unlike-sign (blue) pions (left) and protons (right) in Au+Au collisions at 30%-40% centrality and eight different energies from 7.7 GeV (top left) to 200 GeV (bottom right). Also shown at the highest beam energies in the right frames are the antiproton-antiproton correlations.

$(\Delta y, \Delta\varphi)$ (compared to that for the the unlike-sign pairs) which was shown in Fig. 2. The correlations of the like-sign pions and protons (red) are larger than those for the unlike-sign pairs (blue) on the away-side.

The Δy dependence of the correlations on the near-side explored in Fig. 4 come into better focus when requiring each pair is also on the near-side azimuthally, and are shown in Fig. 5. Here, the correlations of the unlike-sign pions is larger than those for like-sign pairs, which is opposite to the behavior observed on the away-side. The near-side proton correlations shown in Fig. 5b indicate an anticorrelation in both the like-sign and unlike-sign charge combinations. Here it is again seen, as in Fig. 2, that the unlike-sign proton anticorrelation is much narrower in Δy compared to that for the like-sign proton pairs.

The unlike-sign pion correlations shown in Fig. 5a are much wider on the near side (left frames) in Δy than those for the like-sign pion pairs. This is presumably due to local charge conservation in unlike-sign pairs [35]. The effects of local charge conservation on the proton correlations is less clear, but the difference of the unlike-sign and like-sign correlation functions are similar for both pions and protons at the larger values of Δy. Therefore, local charge conservation may contribute to the faster rise in the unlike-sign proton correlations compared to the like-sign pairs.

The measured pion and proton correlation functions were compared to those obtained using the events generated by several model event generators. The analysis was done for simulated events using UrQMD v3.4 [17], Hijing v1.411 [18], and AMPT v2.26t7b [19]. The UrQMD model is based on the covariant propagation of color strings, constituent quarks, and diquarks accompanied by mesonic and baryonic degrees of freedom. It simulates multiple interactions of ingoing and newly produced particles, the excitation and fragmentation of color strings, and the formation and decay of hadronic resonances [17]. The Hijing model is used to study jet and multiparticle production in high energy p+p, p+A, and A+A collisions at RHIC and LHC energies. The model includes multiple minijet production, nuclear shadowing of the

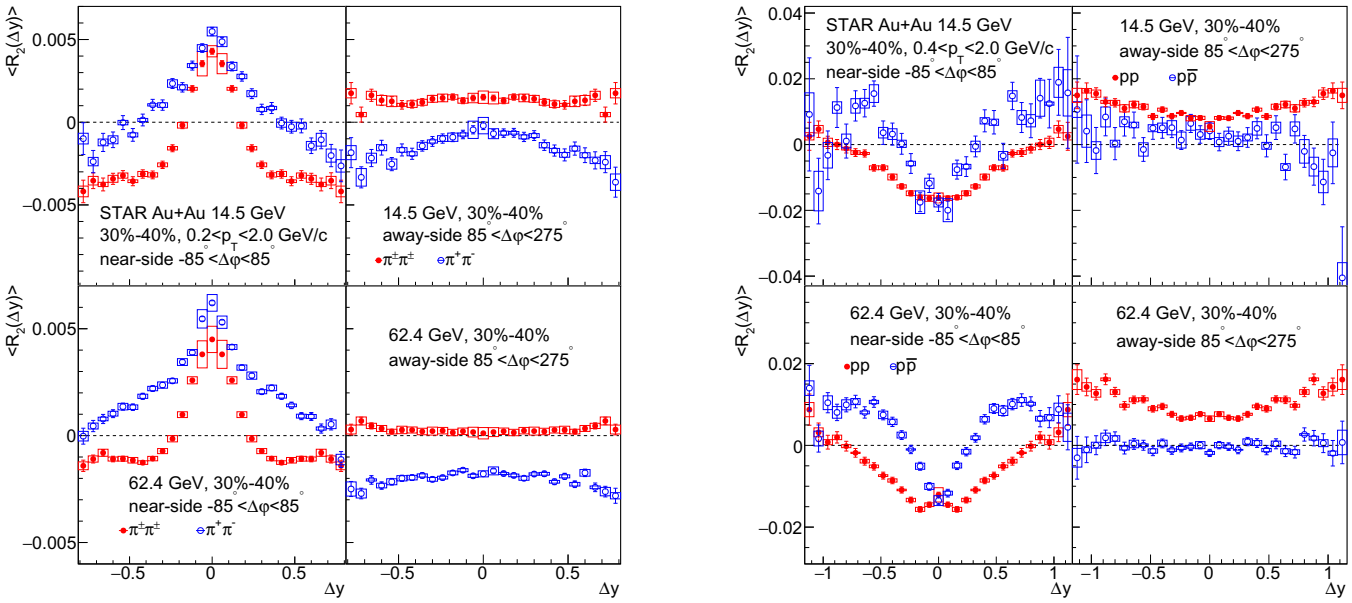

(a) pions (b) protons

FIG. 5: Near-side and away-side $\langle R_2(\Delta y)\rangle$ projection of like-sign (red) and unlike-sign (blue) pions (left) and protons (right) in Au+Au collisions at 14.5 GeV (top) and 62.4 GeV (bottom), 30%-40% centrality.

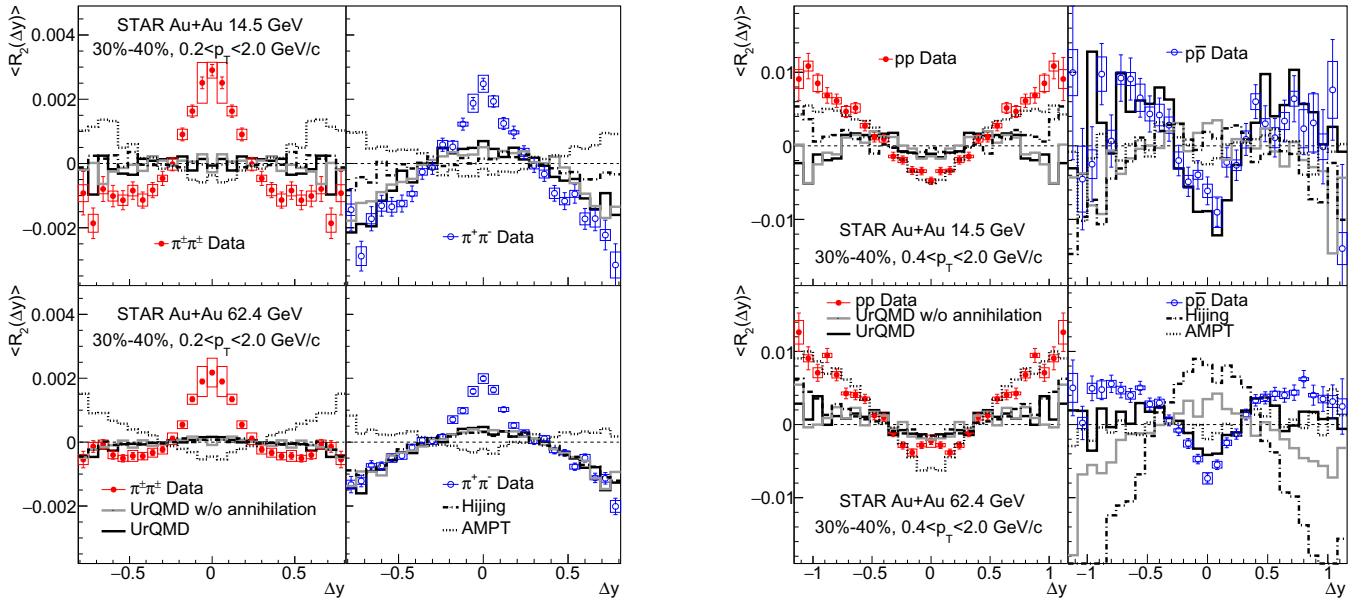

(a) pions (b) protons

FIG. 6: Projection of correlation function $\langle R_2(\Delta y)\rangle$ of like-sign (red) and unlike-sign (blue) pions (left) and protons (right) in Au+Au collisions at 14.5 GeV (top) and 62.4 GeV (bottom), 30%-40% centrality compared with the UrQMD (solid line), Hijing (dash-dotted line), and AMPT (dotted line) simulations.

parton distribution functions, and a schematic mechanism of jet interactions in dense matter, which contains many sources of long and short-range correlations [18]. A "multi-phase transport model," (AMPT) uses the Hijing model for generating the initial conditions, then models the partonic scattering, string fragmentation using the Lund model, hadronization via quark coalescence, and finally hadronic rescattering [19].

Approximately 30M minimum bias events were generated using the default parameters for each model. Addi-

tional model data sets of the same significance were also generated following the modification of specific model parameters in order to further explore specific topics. The centrality of the model events was determined by integrating the minimum bias distributions of the charged particle multiplicities calculated with the same kinematic cuts as were used for the analysis of the experimental data.

Figure 6 depicts the comparison of the experimental and model results for like-sign and unlike-sign pions and protons at 14.5 GeV and 62.4 GeV in 30%-40% mid-central collisions. None of the three models describes the observed pion correlations at small values of the rapidity difference, Δy. As described above, this strong short range peak in the like sign correlations appears to be predominantly femtoscopic in origin as it can be removed by removing pairs with $\Delta q < 100$ MeV/c. This can be expected as the models generally make no attempt to describe femtoscopy in their default configurations. However, the disagreement between the data and models for the unlike-sign pion short-range correlations cannot be explained by femtoscopy as the same Δq cut does not remove the short-range correlation, and the particles in the pair are distinguishable.

The UrQMD and Hijing models were more successful than AMPT in reproducing the correlations of unlike-sign pions at larger values of Δy. This may be the result of a stricter local charge conservation in UrQMD and Hijing compared to AMPT [36].

For the proton correlations, Hijing does not describe the data, while UrQMD and AMPT qualitatively predict a small suppression near $\Delta y \sim 0$ of like-sign and unlike-sign protons, respectively, but do not reproduce the observed correlations at larger values of Δy. The AMPT model can reproduce the observed anticorrelations for like-sign protons (but fails for unlike-sign protons), while the UrQMD model can describe the unlike-sign protons (but fails for like-sign protons).

Also shown in Fig. 6 are the results from UrQMD when baryon annihilation is turned off via a user parameter[1]. The unlike-sign proton correlations in these events now no longer reproduce those seen in the data near $\Delta y \sim 0$, and in fact they look quite similar to those obtained from Hijing and AMPT. This suggests that the anticorrelation in unlike-sign proton pairs on the near side in $\Delta\varphi$ and at short range in Δy, best seen in the right frames of Fig. 2, results from baryon-antibaryon annihilation.

The anticorrelation in like-sign protons is broader and longer range. Similar two-proton anticorrelations (see also Ref. [37]) were reported in the small collision system of e^++e^- annihilation at $\sqrt{s} = 29$ GeV by the TPC/Two-Gamma Collaboration [38], and in p+p collisions at $\sqrt{s} = 7$ TeV by the ALICE Collaboration [39]. We report this observation here for the first time in the large collision system of Au+Au. Although there is a qualitative similarity in the (anti)correlations of like-sign protons between the small and large systems, there is no such agreement for unlike-sign protons.

The observed proton anticorrelations in e^++e^- annihilation at $\sqrt{s} = 29$ GeV were suggested [38] to result from local baryon number conservation during the hadronization process and the "energy cost" required to produce two baryons during the fragmentation of a single string. According to the string hadronization model [40], two baryons produced in a single fragmentation should be separated by at least one particle with a different baryon number [38, 39]. Furthermore, the probability of producing two baryons in a single fragmentation in low energies is suppressed, since a minimum of two baryons and two antibaryons would be required to produce two like-sign baryons while conserving baryon number. This explanation could be reasonable at the low beam energy of 29 GeV. However, such an energy constraint seems unlikely in the case of the p+p collisions at $\sqrt{s} = 7$ TeV measured by ALICE, which showed a similar near-side suppression. In the ALICE study [39], the possibility that the like-sign proton correlations were suppressed on the near-side by Fermi-Dirac statistics was ruled out as the pΛ+$\bar{\text{p}}\bar{\Lambda}$ correlators also showed the same anticorrelations. Other ideas like the effects of the momentum transfer during the interaction, Coulomb repulsion, local baryon number conservation, and energy conservation were also discussed in Ref. [39], but none of these were seen as entirely successful in explaining their observed baryon anticorrelations.

The pion and proton correlations were studied in different centralities from the most central to the most peripheral collisions. The results of the most central 0%-5%, mid-central 30%-40%, and peripheral 60%-70% events in Au+Au collisions at the low energy of 14.5 GeV, and the higher energy of 62.4 GeV, are shown in Fig. 7. A strong centrality dependence is observed in the pion and proton correlations. In both cases, the (anti)correlations decrease, *i.e.*, R_2 approaches zero from above or below, as the collisions become more central. This is consistent with the usual picture of the dilution of the correlations due to the increasing number of particle sources as the collisions become more central.

These correlations were also studied in two different transverse momentum ranges. The low-p_T range for pions and protons was 0.2-0.6 GeV/c and 0.4-0.8 GeV/c, respectively, while the high-p_T range for pions and protons was 0.6-2.0 GeV/c and 0.8-2.0 GeV/c, respectively. In Fig. 8, the pion and proton correlations in these two p_T ranges are shown for 30%-40% mid-central collisions at 14.5 GeV and 62.4 GeV. The proton correlations show no significant dependence on the transverse momentum range for both the unlike- and like-sign charge combinations. There is a more significant p_T dependence for the like-sign pion correlations at large Δy, while the unlike-sign pions do not show a significant p_T dependence.

The influence of femtoscopic correlations on the observed proton anticorrelations was also studied. A rela-

[1] UrQMD "CTOption(19)" was changed from zero to one.

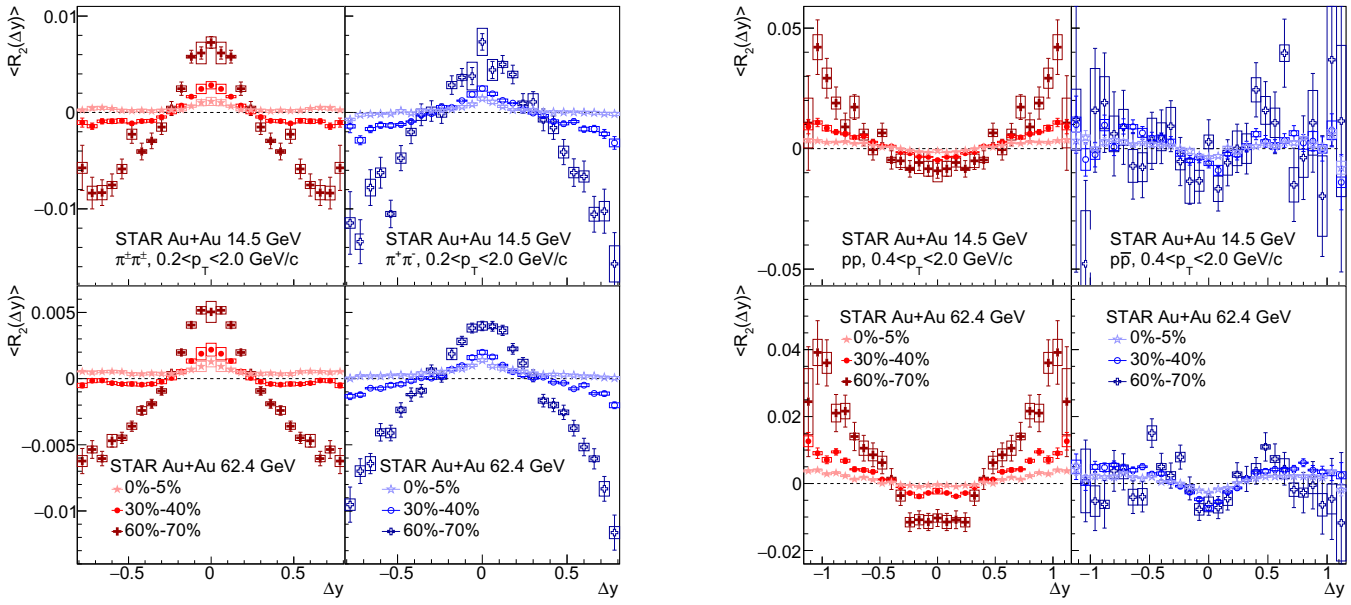

(a) pions (b) protons

FIG. 7: Projection of correlation function $\langle R_2(\Delta y)\rangle$ of like-sign (red) and unlike-sign (blue) pions (left) and protons (right) in Au+Au collisions at 14.5 GeV (top) and 62.4 GeV (bottom) for the most central 0%-5%, mid-central 30%-40% and peripheral 60%-70% events.

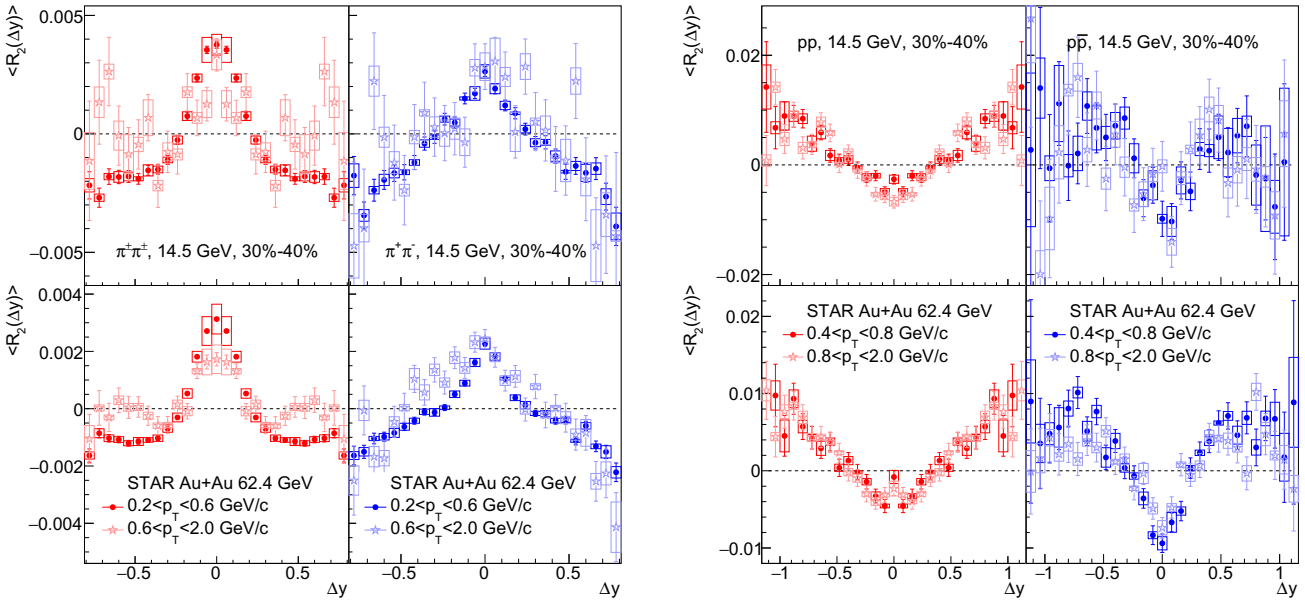

(a) pions (b) protons

FIG. 8: Projection of correlation function $\langle R_2(\Delta y)\rangle$ of like-sign (red) and unlike-sign (blue) pions (left) and protons (right) in low and high p_T in Au+Au collisions at 14.5 GeV (top) and 62.4 GeV (bottom) in 30%-40% centrality.

tive invariant momentum cut was set based on the values of the effective source size measured by STAR [41, 42]. This cut would be expected to suppress all femtoscopic contributions. The bins of the correlation function affected by such a cut is limited to the rather small region of $\Delta y < 0.1$. This is much narrower than the observed width of the observed proton anticorrelations.

IV. SUMMARY AND CONCLUSIONS

The two-particle angular correlation functions were studied for like-sign and unlike-sign pion, kaon, and proton pairs in the Beam Energy Scan data collected by the STAR experiment. The energy, centrality, and p_T dependence of the correlations were investigated. No nonmonotonic behavior was observed in any of the two-particle angular correlation functions as a function of the beam energy from 7.7 to 200 GeV and indeed the dependence on the beam energy is quite weak overall. The experimental results were also compared to those obtained from the models UrQMD, Hijing, and AMPT.

The expected near-side peak was observed in the pion and kaon correlations which is associated with short-range mechanisms. In the case of the like-sign two-pion correlations, this peak appears to be predominantly femtoscopic in the kinematic range of this analysis as it can be removed by removing pairs with a relative four-vector difference of less than 100 MeV/c. The amplitudes of the correlations decrease with increasing beam energy and decrease as the collisions become more central, and are at most weakly dependent on the transverse momentum in two wide bins of this variable. A strong near-side ring-shaped positive correlation was observed in the unlike-sign kaon correlations resulting from the strongly correlated pairs from $\phi(1020)$ decays.

In contrast to the meson correlations, the proton pairs exhibit a significant near-side anticorrelation at all beam energies. This proton anticorrelation has already been observed in small systems and is here reported for the first time in the large collision system of Au+Au. This anticorrelation was observed in both like-sign and unlike-sign (anti)proton pairs, and it is wider in relative rapidity, Δy, for the like-sign charge combination as compared to the unlike-sign combination. The model comparisons imply that the anticorrelation in the unlike-sign proton pairs is caused by baryon-antibaryon annihilation. A description of the cause of the stronger and longer-range anticorrelation in the like-sign proton pairs is not yet in hand. This like-sign proton anticorrelation is apparently p_T-independent, decreasing with increasing beam energy, and decreasing as the collisions become more central.

ACKNOWLEDGMENTS

We thank the RHIC Operations Group and RCF at BNL, the NERSC Center at LBNL, and the Open Science Grid consortium for providing resources and support. This work was supported in part by the Office of Nuclear Physics within the U.S. DOE Office of Science, the U.S. National Science Foundation, the Ministry of Education and Science of the Russian Federation, National Natural Science Foundation of China, Chinese Academy of Science, the Ministry of Science and Technology of China and the Chinese Ministry of Education, the National Research Foundation of Korea, Czech Science Foundation and Ministry of Education, Youth and Sports of the Czech Republic, Hungarian National Research, Development and Innovation Office, New National Excellency Programme of the Hungarian Ministry of Human Capacities, Department of Atomic Energy and Department of Science and Technology of the Government of India, the National Science Centre of Poland, the Ministry of Science, Education and Sports of the Republic of Croatia, RosAtom of Russia and German Bundesministerium fur Bildung, Wissenschaft, Forschung and Technologie (BMBF) and the Helmholtz Association.

[1] L. Foá, Phys. Rept. **22**, 1 (1975).
[2] E. A. De Wolf, I. M. Dremin, and W. Kittel, Phys. Rept. **270**, 1 (1996), arXiv:hep-ph/9508325 [hep-ph].
[3] K. Eggert *et al.*, Nucl. Phys. **B86**, 201 (1975).
[4] R. E. Ansorge *et al.* (UA5 Collaboration), Z. Phys. **C37**, 191 (1988).
[5] M. Connors, C. Nattrass, R. Reed, and S. Salur, Rev. Mod. Phys. **90**, 025005 (2018), arXiv:1705.01974 [nucl-ex].
[6] M. A. Lisa, S. Pratt, R. Soltz, and U. Wiedemann, Annu. Rev. Nucl. Part. Sci. **55**, 357 (2005), arXiv:0505014 [nucl-ex].
[7] G. Aad *et al.* (ATLAS Collaboration), Phys. Rev. **C86**, 014907 (2012), arXiv:1203.3087 [hep-ex].
[8] N. Borghini, P. M. Dinh, J.-Y. Ollitrault, A. M. Poskanzer, and S. A. Voloshin, Phys. Rev. **C66**, 014901 (2002), arXiv:nucl-th/0202013 [nucl-th].
[9] N. Borghini, P. M. Dinh, and J.-Y. Ollitrault, Phys. Rev. **C62**, 034902 (2000), arXiv:nucl-th/0004026 [nucl-th].
[10] Y. Hatta and M. A. Stephanov, Phys. Rev. Lett. **91**, 102003 (2003), [Erratum: Phys. Rev. Lett. **91**, 129901 (2003)], arXiv:hep-ph/0302002 [hep-ph].
[11] M. A. Stephanov, K. Rajagopal, and E. V. Shuryak, Phys. Rev. Lett. **81**, 4816 (1998), arXiv:hep-ph/9806219 [hep-ph].
[12] M. A. Stephanov, K. Rajagopal, and E. V. Shuryak, Phys. Rev. **D60**, 114028 (1999), arXiv:hep-ph/9903292 [hep-ph].
[13] M. A. Stephanov, Phys. Rev. **D65**, 096008 (2002), arXiv:hep-ph/0110077 [hep-ph].
[14] N. G. Antoniou, F. K. Diakonos, and A. S. Kapoyannis, in *From e^+e^- to Heavy Ion Collisions: Proceedings of the 30th International Symposium on Multiparticle Dynamics (ISMD 2000), Tihany, Hungary, October 9-15, 2000* (2001) pp. 410–416, arXiv:hep-ph/0102263 [hep-ph].
[15] V. Koch, M. Bleicher, and S. Jeon, *Statistical QCD. Proceedings, International Symposium, Bielefeld, Germany, August 26-30, 2001*, Nucl. Phys. **A698**, 261 (2002), [Nucl. Phys.A702,291(2002)], arXiv:nucl-th/0103084 [nucl-th].
[16] C. Pruneau, S. Gavin, and S. Voloshin, Phys. Rev. **C66**, 044904 (2002), arXiv:nucl-ex/0204011 [nucl-ex].

[17] S. A. Bass *et al.*, Prog. Part. Nucl. Phys. **41**, 255 (1998), arXiv:nucl-th/9803035 [nucl-th].

[18] X.-N. Wang and M. Gyulassy, Phys. Rev. **D44**, 3501 (1991).

[19] Z.-W. Lin, C. M. Ko, B.-A. Li, B. Zhang, and S. Pal, Phys. Rev. **C72**, 064901 (2005), arXiv:nucl-th/0411110 [nucl-th].

[20] M. Anderson *et al.*, Nucl. Instrum. Meth. **A499**, 659 (2003), arXiv:nucl-ex/0301015 [nucl-ex].

[21] W. J. Llope (STAR Collaboration), Nucl. Instrum. Meth. **A661**, S110 (2012).

[22] M. A. Green, IEEE transactions on applied superconductivity **3**, 104 (1993).

[23] W. J. Llope *et al.*, Nucl. Instrum. Meth. **A759**, 23 (2014), arXiv:1403.6855 [physics.ins-det].

[24] E. G. Judd *et al.*, Nucl. Instrum. Meth. **A902**, 228 (2018).

[25] L. Tarini (STAR Collaboration), Ph.D. thesis, Wayne State University (2011).

[26] M. L. Miller, K. Reygers, S. J. Sanders, and P. Steinberg, Ann. Rev. Nucl. Part. Sci. **57**, 205 (2007), arXiv:nucl-ex/0701025 [nucl-ex].

[27] M. M. Aggarwal *et al.* (STAR Collaboration), Phys. Rev. Lett. **105**, 022302 (2010), arXiv:1004.4959 [nucl-ex].

[28] L. Adamczyk *et al.* (STAR Collaboration), Phys. Rev. Lett. **113**, 092301 (2014), arXiv:1402.1558 [nucl-ex].

[29] L. Adamczyk *et al.* (STAR Collaboration), Phys. Lett. **B785**, 551 (2018), arXiv:1709.00773 [nucl-ex].

[30] S. Ravan, P. Pujahari, S. Prasad, and C. A. Pruneau, Phys. Rev. **C89**, 024906 (2014), arXiv:1311.3915 [nucl-ex].

[31] W. Kittel, *Proceedings, 34th International Symposium on Multiparticle dynamics (ISMD 2004): Rohnert Park, USA, July 26-August 1, 2004*, Acta Phys. Polon. **B36**, 291 (2005).

[32] W. Kittel, in *Multiparticle dynamics. Proceedings, 31st International Symposium, ISMD 2001, Datong, China, September 1-7, 2001* (2001) pp. 298–306, arXiv:hep-ph/0111462 [hep-ph].

[33] C. Patrignani *et al.* (Particle Data Group), Chin. Phys. **C40**, 100001 (2016).

[34] B. I. Abelev *et al.* (STAR Collaboration), Phys. Rev. **C79**, 064903 (2009), arXiv:0809.4737 [nucl-ex].

[35] P. Bozek and W. Broniowski, Phys. Rev. Lett. **109**, 062301 (2012), arXiv:1204.3580 [nucl-th].

[36] X. Pan, F. Zhang, Z. Li, L. Chen, M. Xu, and Y. Wu, Phys. Rev. **C89**, 014904 (2014), arXiv:1311.0948 [nucl-th].

[37] P. Bhattarai, Ph.D. Thesis, University of Texas - Austin (2016).

[38] H. Aihara *et al.* (TPC/Two Gamma Collaboration), Phys. Rev. Lett. **57**, 3140 (1986).

[39] J. Adam *et al.* (ALICE Collaboration), Eur. Phys. J. **C77**, 569 (2017), arXiv:1612.08975 [nucl-ex].

[40] B. Andersson, in *Proceedings of the 7th European Symposium on Antiproton Interactions: From LEAR to the Collider and Beyond, Durham, England* (1986) pp. 447–462.

[41] S. Siejka (STAR Collaboration), Nucl. Phys. **A982**, 359 (2019).

[42] L. Adamczyk *et al.* (STAR Collaboration), Phys. Rev. **C92**, 014904 (2015), arXiv:1403.4972 [nucl-ex].